

IAC-19,C1,1,3,x50777

## Concepts and Applications of Aerodynamic Attitude and Orbital Control for Spacecraft in Very Low Earth Orbit

Sabrina Livadiotti<sup>a\*</sup>, Nicholas H. Crisp<sup>b</sup>, Peter C.E. Roberts<sup>a</sup>, Steve Edmondson<sup>a</sup>, Sarah J. Haigh<sup>a</sup>, Claire Huyton<sup>a</sup>, Rachel E. Lyons<sup>a</sup>, Vitor T.A. Oiko<sup>a</sup>, Katharine L. Smith<sup>a</sup>, Luciana A. Sinpetru<sup>a</sup>, Alastair Straker<sup>a</sup>, Stephen D. Worrall<sup>a</sup>, Jonathan Becedas<sup>b</sup>, Rosa María Domínguez<sup>b</sup>, David González<sup>b</sup>, Valentín Cañas<sup>b</sup>, Virginia Hanessian<sup>c</sup>, Anders Mølgaard<sup>c</sup>, Jens Nielsen<sup>c</sup>, Morten Bisgaard<sup>c</sup>, Adam Boxberger<sup>d</sup>, Yung-An Chan<sup>d</sup>, Georg H. Herdrich<sup>d</sup>, Francesco Romano<sup>d</sup>, Stefanos Fasoulas<sup>d</sup>, Constantin Traub<sup>d</sup>, Daniel Garcia-Almiñana<sup>e</sup>, Silvia Rodríguez-Donaire<sup>e</sup>, Miquel Sureda<sup>e</sup>, Dhiren Kataria<sup>f</sup>, Ron Outlaw<sup>g</sup>, Badia Belkouchi<sup>h</sup>, Alexis Conte<sup>h</sup>, Jose Santiago Perez<sup>h</sup>, Rachel Villain<sup>h</sup>, Barbara Heißerer<sup>i</sup> and Ameli Schwalber<sup>i</sup>

<sup>a</sup> The University of Manchester, Oxford Road, Manchester, M13 9PL, United Kingdom

<sup>b</sup> Elecnor Deimos Satellite Systems, Calle Francia 9, 13500 Puertollano, Spain

<sup>c</sup> GomSpace AS, Langagervej 6, 9220 Aalborg East, Denmark

<sup>d</sup> University of Stuttgart, Pfaffenwaldring 29, 70569 Stuttgart, Germany

<sup>e</sup> UPC-BarcelonaTECH, Carrer de Colom 11, 08222 Terrassa, Barcelona, Spain

<sup>f</sup> Mullard Space Science Laboratory (UCL), Holmbury St. Mary, Dorking, RH5 6NT, United Kingdom

<sup>g</sup> Christopher Newport University Engineering, Newport News, Virginia 23606, United States

<sup>h</sup> Euroconsult, 86 Boulevard de Sébastopol, 75003 Paris, France

<sup>i</sup> concentris research management gmbh, Ludwigstraße 4, D-82256 Fürstentfeldbruck, Germany

\* Corresponding Author: [sabrina.livadiotti@manchester.ac.uk](mailto:sabrina.livadiotti@manchester.ac.uk)

### Abstract

Spacecraft operations below 450km, namely Very Low Earth Orbit (VLEO), can offer significant advantages over traditional low Earth orbits, for example enhanced ground resolution for Earth observation, improved communications latency and link budget, or improved signal-to-noise ratio. Recently, these lower orbits have begun to be exploited as a result of technology development, particularly component miniaturisation and cost-reduction, and concerns over the increasing debris population in commercially exploited orbits. However, the high cost of orbital launch and challenges associated with atmospheric drag, causing orbital decay and eventually re-entry are still a key barrier to their wider use for large commercial and civil spacecraft. Efforts to address the impact of aerodynamic drag are being sought through the development of novel drag-compensation propulsion systems and identification of materials which can reduce aerodynamic drag by specularly reflecting the incident gas. However, the presence of aerodynamic forces can also be utilised to augment or improve spacecraft operations at these very low altitudes by providing the capability to perform coarse pointing control and trim or internal momentum management for example. This paper presents concepts for the advantageous use of spacecraft aerodynamics developed as part of DISCOVERER, a Horizon 2020 funded project with the aim to revolutionise Earth observation satellite operations in VLEO. The combination of novel spacecraft geometries and use of aerodynamic control methods are explored, demonstrating the potential for a new generation of Earth observation satellites operating at lower altitudes.

**Keywords:** VLEO, aerodynamic attitude control, orbital aerodynamics, free molecular flow

### 1. Introduction

In the last few decades, the meaningful progress made in microsatellites development have encouraged the employment of a new generation of cost effective platforms for a range of scientific applications. However, the constraints imposed on mass, dimensions and power requirements pose a challenge especially with regards to the design of the attitude and the orbit control systems. Traditional attitude control dedicated actuators such as reaction wheels (RWs) need to be properly scaled, with consequent performance degradation due to decrease in wheel radius [2]. Reduced space allocations impose some

limitations on the design of the propulsion systems as well as on the amount of fuel transportable, with obvious impact on the mission lifetime. For these reasons, the investigation of alternative cost-effective attitude and orbit control techniques taking advantage of the environmental torques experienced by the satellite in orbit appears to be justified.

DISCOVERER is a Horizon 2020 research project which, among others, aspires to investigate and prove the feasibility of aerodynamic control methods for attitude and orbit control in VLEO, i.e. below 450 km. In particular, the implementation and on-orbit demonstration of a proposed selection of aerodynamic

attitude control manoeuvres on SOAR - a 3U CubeSat satellite scheduled to be launched in 2020 - constitute secondary objectives of the mission [1].

Aerostability in pitch and yaw, i.e. passive aerodynamic static stabilisation, was investigated [3]–[8] and successfully demonstrated in orbit [9]–[11]. Feasibility of aerodynamic attitude and pointing manoeuvring finds some precedents in literature [12]–[16]. However, more complex implementations of control techniques seem to be rarer and on-orbit demonstration is still to be achieved. Gargasz [12] considered feasibility of three-axes active aerodynamic attitude control for an aerostable configuration characterised by four independent control panels mounted at the rear of a cubical main body. Three-axis attitude control was also studied by Llop in [13] for a feathered CubeSat configuration. Auret and Steyn [14] investigated a synergetic implementation of an aerodynamic roll control and a magnetic attitude control scheme for a 3U CubeSat. Hao and Roberts [15] developed an optimal energetically modified B-dot control algorithm to remove satellite’s librational motion through a combined use of aerodynamic and magnetic control. A preliminary feasibility study focused on the aerodynamic dumping of the momentum stored in the RWs was proposed by Mostaza-Prieto in [16].

The use of differential aerodynamic forces for orbit manoeuvring and control received much wider attention in literature. The majority of the works discuss a possible employment of aerodynamic drag accelerations to perform rendezvous [17]–[19], formation-keeping [20]–[22] and deployment [23] and atmospheric interface re-entry targeting [24], [25]. Investigations regarding a combined use of drag, lift and side-force to achieve orbit control are rarer [26]–[29] but relevant for satellites characterise by stabilised attitude [30]. Recent contribution to the discussion were provided by DISCOVERER in [31].

Given these premises, the objective of this study is to discuss preliminary results obtained in investigating the feasibility of aerodynamic attitude control techniques for varying initial orbital conditions and satellite geometries. In these regards, the purpose is to show the range of applicability of these manoeuvres rather than perform a trade-off study. The use of aerodynamic actuators was considered to perform combined aerodynamic and RWs pointing, aerodynamic management of the momentum stored in the RWs and aerodynamic trim. After a brief description of the simulation environment employed and the assumptions made, the results referring to the implementation of these manoeuvres for the selected geometries are discussed.

## 2. Aerodynamic Control Implementation and Platforms Design

### 2.1. Platforms Concepts

The performance achievable employing orbital aerodynamics for attitude control tasks not only rely on a proper design and implementation of the controller but also on the platform employed. In this study, two aerostable configurations and a neutrally stable configuration were considered.

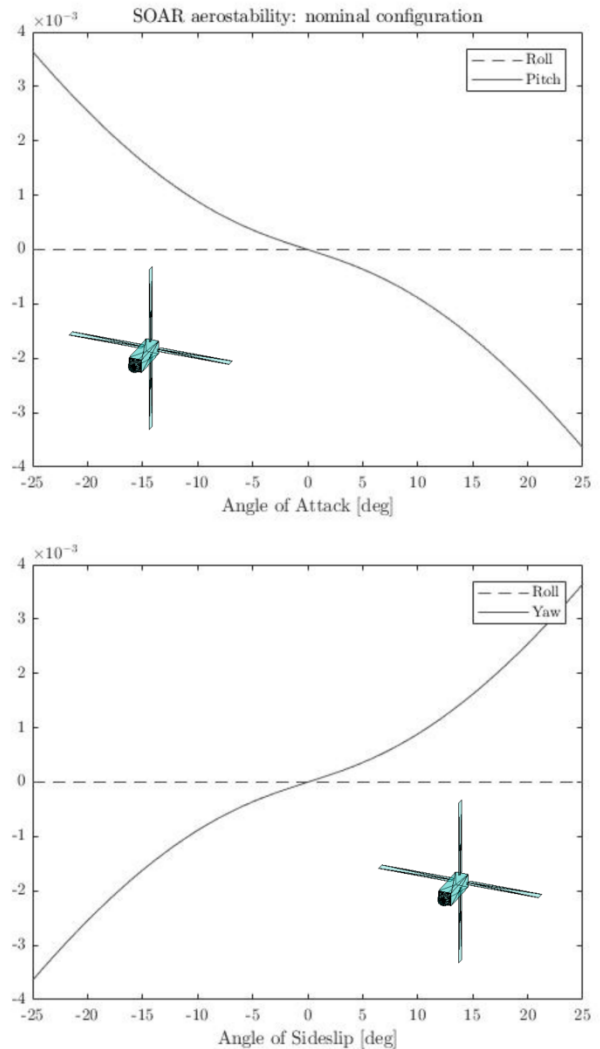


Figure 1: Aerostability characteristic in roll, pitch and yaw for SOAR (aerostable feathered geometry) in its nominal configuration.

SOAR (Figure 1) is an example of a nominally aerostable feathered configuration [32]. Four aerodynamic control panels extend at the rear of a 3U CubeSat main body. The relative offset between the centre of Mass (CoM) and the aerodynamic Centre of Pressure (CoP) is such that aerostability in pitch and yaw axes is assured (Figure 1). Nominally aerostable geometries naturally induce aerodynamic restoring torques when their attitude is perturbed, thus granting static stability. For fixed aerostable configurations, however, the magnitude of the

aerodynamic torques is not big enough to damp residual rates. As a consequence the satellite persistently oscillates about the incoming flow direction. The four panels can be actuated independently: counter-rotation of an opposed set of fins induces a torque about the roll axis. Conversely, panels' co-rotation and asymmetries in the geometry exposed to the flow promote the generation of aerodynamic torques in pitch and yaw. These features make this geometry particularly suited for control and manoeuvring in three axes.

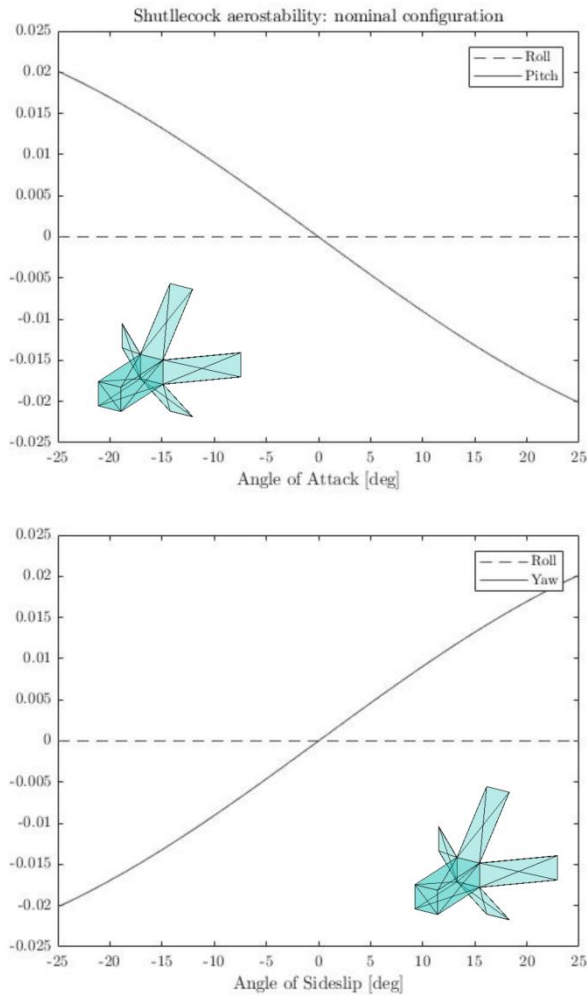


Figure 2: Aerostability characteristic of the aerostable shuttlecock geometry about the roll, pitch and yaw axes in its nominal configuration.

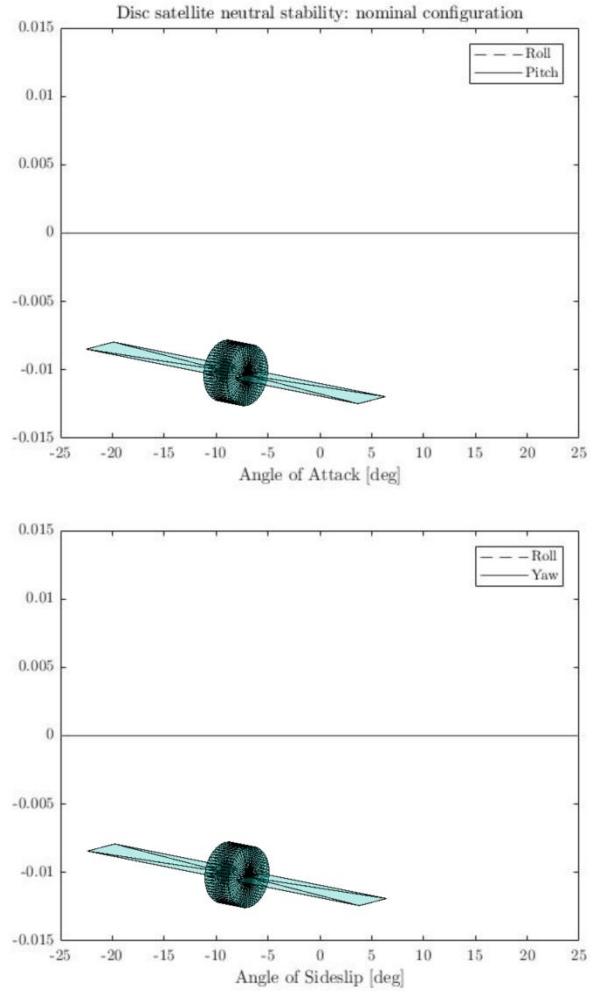


Figure 3: Neutrally stable characteristic in roll, pitch and yaw for the disc satellite in its nominal configuration.

The second geometry investigated is a shuttlecock configuration (Figure 2) endowed with four control surfaces forming an aerostabilising skirt at the rear of a 3U CubeSat main body. Control authority is achieved in pitch and yaw letting each panel rotate about the respective hinge. However, the control action about the roll axis is expected to be limited because of the restrictions imposed on the panels motion.

Table 1: Characteristic dimensions of the three geometries considered.

Dimensions [m]	SOAR	Shuttlecock	Disc Satellite
Panel length	0.58	0.30	0.8
Panel width	0.065	0.10	0.2
Body length	0.30	0.30	0.30
Body width	0.10	0.10	0.15

Finally, a nominally neutrally stable disc satellite configuration was examined (Figure 3). Two opposed control surfaces extend from the side of a cylindrical main body having its lateral surface oriented along the ram direction. The position of these along the main body was selected so that the CoP and the CoM would coincide. In this way, the disturbance torques experienced by the satellite are minimised. Altering the angles of deflection of the panels with regards to the incoming flow causes the loss of the neutrally stable characteristic and permits to achieve some controllability about the roll and yaw axes.

However, aerodynamic control in pitch is not expected to be feasible for this specific configuration since no-offset is present along the longitudinal axis. Characteristic dimensions of the geometries employed are provided in Table 1.

## 2.2. Reference Frames Definition

The reference systems employed for the implementation of the aerodynamic control manoeuvres in the simulation environment are:

*Earth-Centered Inertial (ECI)*: the ECI reference frame is defined in the ecliptic plane of the orbit described by the Earth about the Sun and its origin is coincident with the centre of mass of the Earth. The  $X_I$  axis points towards the vernal equinox, the  $Z_I$  axis is directed along the axis of rotation of the Earth and  $Y_I$  is defined in the ecliptic orbit plane and determined according to the right hand rule. Since the reference system is inertial, the reference frame does not rotate with the Earth.

*Earth-Centered Earth-Fixed (ECEF)*: as for the ECI, the origin of ECEF reference frame is positioned at the centre of mass of the Earth and the frame lies in the ecliptic plane of the Earth's orbit. In this case, however, the motion of the reference frame is integral with the Earth. The  $X_E$  pointing direction is defined by the prime meridian. The  $Z_E$  axis points towards the North Pole and the  $Y_E$  axis is defined according to the right hand rule.

*Local-Vertical Local-Horizontal (LVLH)*: the LVLH reference frame [33] has its origin located at the centre of mass of the satellite and the  $X_{LVLH}$  and the  $Z_{LVLH}$  axes defined in its orbital plane. Specifically, the  $X_{LVLH}$  axis is aligned with the satellite velocity vector direction while the  $Z_{LVLH}$  axis is directed towards the centre of mass of the Earth. The  $Y_{LVLH}$  axis is perpendicular to the orbital plane and it is determined according to the right hand rule.

*Body reference frame*: the body reference frame is centred at the satellite centre of mass and is rigidly fixed to the satellite body. Axes direction definition is here provided assuming initial alignment with LVLH. According to this, the  $X_B$  axis is chosen such that its direction coincides with the velocity vector direction. The  $Z_B$  axis points in nadir to the centre of mass of the

Earth. The  $Y_B$  axis is accordingly derived by means of the right hand rule.

*Flow reference frame*: determination of flow direction is non-negligibly affected by the difficulties encountered in the attempt of determining the vertical component of the thermospheric wind [34]. The level of accuracy achievable is thus limited, but approximated results can be obtained modelling the horizontal wind component. According to this, the flow reference frame was defined with the  $X_F$  axis pointing in the flow direction, the  $Z_F$  axis pointing towards the centre of mass of the Earth and the  $Y_F$  axis pointing along the direction defined by the right hand rule.

*Geocentric Solar Ecliptic (GSE)*: the GSE reference frame has the origin located at the centre of mass of the Earth. The  $X_S$  axis is aligned with the Earth-Sun conjoining line. The  $Z_S$  axis direction is determined computing the cross product between the Earth-Sun vector and the Earth-Sun velocity vector.  $Y_S$  definition follows the right hand rule.

## 2.3. Aerodynamic Manoeuvres Selection

### 2.3.1. Aerodynamic Pointing

A possible employment of aerodynamic torques was evaluated to perform aerodynamic pointing, mainly with regards to the orbital LVLH reference frame. According to the geometry selected, the panels configuration providing the control torque demanded to correct the satellite attitude can be identified and selected. In the following, the feasibility of the manoeuvre was investigated for one axis and two axis aerodynamic attitude control with the remaining axis/axes being controlled by RWs. Two main scenarios are considered for the two aerostable configurations:

1. Combined aerodynamic roll and RWs pitch and yaw control;
2. Combined aerodynamic pitch and yaw control and RWs roll control.

For the neutrally stable configuration, since the design do not allow for the generation of any control torque in pitch, the following manoeuvre was considered:

3. Aerodynamic roll control and RWs pitch and yaw control.

It is important to mention in this context that, especially at higher VLEO altitudes (>300 km) just coarse pointing accuracy is expected to be achievable in the aerodynamic controlled axis. Finer performance can be however achieved combing aerodynamic and conventional actuators.

### 2.3.2. Aerodynamic Trim

Aerodynamic trim refers to a possible employment of the aerodynamic torques induced on the satellite to counteract other external disturbances affecting the plant and keep the satellite in the desired orientation.

Aerodynamic trim was performed for a number of cases study: according to what previously affirmed, the performance achievable were evaluated implementing the manoeuvre after the aerodynamic pointing task was completed and the attitude was coarsely corrected to the desired orientation. For this reason, when aerodynamic pointing manoeuvres are performed, the panels do not come back to the nominal configuration but are still actuated to perform the aerodynamic trim task.

A successful implementation of this manoeuvre is of particular interest since it can relax the actuation effort imposed on traditional control devices (RWs) and limit angular momentum build-up, thus effectively reducing the frequency of desaturation manoeuvres on orbit, especially at lower altitudes.

### 2.3.3. Aerodynamic Momentum Management

Aerodynamic torques can also be employed to manage the angular momentum stored in the RWs and avoid internal actuators saturation. Disturbing environmental torques are characterised by periodic and secular components. While periodic components are characterised by a cyclic variation corresponding to the orbital period, the secular component causes the rates in the actuators to linearly increase, eventually leading to saturation. When this condition occurs the plant can no longer be controlled and the stability of the system is compromised.

Adopting an aerodynamic dumping strategy may prove to have some advantages over more traditional devices usually employed to perform this task, such as magnetorquers. The level of performances achievable with aerodynamic and magnetic dumping is respectively affected by the uncertainties characterising orbital aerodynamics and by an accurate modelling of the Earth's magnetic field. However, aerodynamic dumping authority is not limited to directions that are not perpendicular to the magnetic field of the Earth.

Different performances are expected to be observed with materials employed, variation in the environmental conditions mainly due to solar cycle and altitude. Whilst aerodynamic wheels desaturation appears to be achievable [16], the time required to reduce the momentum in the wheels to an acceptable level to perform attitude control tasks might make this manoeuvre impractical for actual implementation. This is especially true if stringent requirements are imposed on target acquisition.

According to this, a control scheme was implemented to evaluate whether aerodynamic torques could be used to compensate for the angular momentum accumulated in the RWs whilst they are employed to perform attitude control. Simulations were performed for the shuttlecock and the feathered configuration for two different scenarios:

1. Saturation avoidance for off-ram direction target pointing;
2. Saturation avoidance for off-ram direction target pointing and attitude control manoeuvre.

More insights on the controller design for this specific task are provided in Section 3.2.

### 2.4. Simulation Environment

The purpose of this section is to provide some information regarding the simulation environment used to test the aerodynamic control manoeuvres discussed above. These need to be intended as a common ground to the results shown in Section 4. Any variations to what discussed in the current section will be mentioned in the appropriate context.

Fluctuations of the residual atmospheric density [35] are implemented assuming quiet solar magnetic activity, or equivalently, reduced Extremely Ultraviolet (EUV) emissions. Estimation of thermospheric density variations with day-to-night, seasonal-latitudinal, semi-annual and solar cycle variations are difficult to acknowledge with simplified exponential models. For this reason, this work relies on the estimation of the density values provided by the NRLMSISE-00 [36] atmospheric model.

Including the effects of atmospheric circulation is especially important when possible applications of aerodynamic torques for orbital and attitude control are investigated. For non-equatorial orbits, the thermosphere co-rotation with the Earth introduces a disturbance in the satellite attitude motion about the yaw axis that needs to be addressed. Uncertainties in the estimation of the flow direction are introduced by the thermospheric winds, whose generation, velocity and prevailing direction is due to the complex interaction of phenomena occurring in the upper atmosphere, such as gradients of pressure and reduced kinematic viscosity. At the current state of the art, wind models offer a good description of the horizontal components of the wind, while major uncertainties are encountered in the estimation of the vertical components [34]. For the set of simulations discussed in Section 4, the effect of zonal and meridional winds in the determination of the direction of the incoming flow was modelled with the HWM-93 [37]–[39] model, as suggested in the ECSS Space Environment standard [40].

The satellite dynamics and kinematics are affected by environmental disturbances torques and forces which have an impact on the design and on the robustness of the controller. Solar radiation pressure, gravity gradient and undesired aerodynamic torques and accelerations are for this reason included in the simulation environment. Mathematical description of orbital perturbation effects due to the non-uniform Earth's gravitational field are included considering zonal harmonics up to the fourth degree ( $J_4$ ). Solar radiation pressure torques and accelerations produced by the interaction of solar

radiation with the exposed surfaces is modelled adopting specular and diffuse reflectivity coefficients of 0.15 and 0.25, respectively. The total disturbances are evaluated, for the current configuration, implementing a panel method through a mesh discretisation and summing the contributions computed for each surface. In this way, the robustness of the controllers could also be tested against variations in the disturbance torques experienced by the satellite between periods of eclipse.

Given a defined geometry, the aerodynamic control authority achievable by surface actuation is dependent on the model employed to provide a physical description of the mechanisms of interaction occurring between gas particles and surface atoms [41]. For a given gas-surface interaction (GSI) model, the induced aerodynamic torques and forces in roll, pitch and yaw vary with the thermal or the momentum accommodation coefficients. According to this, the materials that constitute the surface exposed to the flow have an impact on the expected aerodynamic performances. For this study, Sentman's model [42] is employed with high thermal accommodation coefficients ( $\alpha$ ) to represent the behaviour and the performance expected to be achievable at the current state of the art. In particular,  $\alpha$  is assumed to vary in the range 0.9-1 according to reductions of atomic oxygen concentration with decreasing altitude [43], [44].

The aerodynamic control authority exerted by the panels is also limited by eventual shadowing from the incoming flow occurring especially at high orbital inclinations. The impact of this last effect is however likely to be negligible if compared to other source of uncertainties affecting the problem of orbital aerodynamic torques estimation (e.g. reference area definition, aerodynamic coefficients estimation, accuracy of atmospheric and GSI models employed, accommodation coefficients estimation and variation with surface contamination, properties and altitudes). According to this, as a first approximation panels shadowing was neglected but a more rigorous analysis would require its inclusion. In this regard, uncertainties in the aerodynamic control torques produced in output were taken into account through the introduction of an error function to test the robustness of the controller against uncertainties.

### 3. Control Strategy

#### 3.1. Quaternion Feedback Proportional-Integral-Derivative (PID) Control

Combined RWs and aerodynamic attitude control was implemented adopting the quaternion feedback PID control strategy proposed by Bang et al. [45] as a further development of Wie et al. [46] quaternion feedback controller. The PID form of the control law was preferred

over the original proposal [46] because the presence of the integral term permits to reduce the steady-state error and achieve better performances in the presence of external disturbances. The continuous time control law is given by [45]:

$$\vec{u} = \gamma \vec{\omega} \times \vec{H} - K_p \vec{q}_e - K_D \vec{\omega} - K_I \vec{\xi} \quad (1)$$

Where  $\vec{u}$  is the control signal,  $K_p, K_D, K_I$  are the constant proportional, derivative and integral gains,  $\gamma$  is a positive constant gain determining to which extent the cross-coupling gyroscopic term is corrected,  $\vec{\omega}$  is the vector of satellite angular velocity,  $\vec{H}$  is the total angular momentum of the platform,  $\vec{q}_e$  is the quaternion error and  $\vec{\xi}$  is the integral signal. The value of this last is determined introducing a non-linear *intelligent integrator* block. This feature was implemented by the authors [45] to prevent actuators from saturating in the presence of large integral errors. Even though just small angle manoeuvring is considered in this study, the implementation of the intelligent integrator logic proved to be advantageous because of the reduced control authority of the RWs. More details about the controller logic development can be found in the original publication from the authors [45].

The values of  $K_p, K_D, K_I$  were determined using a Linear Quadratic Regulator (LQR) and properly selecting the values of the matrix penalising the state variables and the control signal to include limitations due to actuators saturation. The value of  $\gamma$  was selected to be equal to 1, so that the control signal is accordingly generated to compensate for the gyroscopic term in its entirety. The controller described by Eq. 1 was modified for digital implementation considering a sampling frequency of 1 Hz. The discrete-time formulation was derived applying backwards differentiation and implementing the algorithm according to an incremental/velocity formulation.

#### 3.2. Linear Quadratic Regulator (LQR)

For the angular momentum management task, an infinite-horizon LQR feedback loop is added to the control scheme. The optimal control law is given by:

$$u(t) = -Kx \quad (2)$$

where  $K$  is the optimal gain matrix corresponding to the minimum of a defined performance index  $J$  and  $x$  is the vector of state variables. Given the linear state space model for the system:

$$\dot{x}(t) = Ax(t) + Bu(t) \quad (3)$$

For the infinite-horizon problem the cost function to be minimised does not present any terminal constraint, so that in its discrete time formulation:

$$J = \sum_{k=0}^{\infty} (x_k^T Q x_k + u_k^T R u_k) \quad (4)$$

where  $Q \geq 0$  and  $R > 0$  are symmetric positive semi-definite penalty matrices. Specifically,  $Q$  penalises the state variables and  $R$  the control signal. Since the momentum control loop operates in parallel to the quaternion feedback PID controlling the satellite attitude, it must be designed so that the two loops are characterised by wide separation in frequency or, equivalently, time response. In this way, the interference of the antagonist momentum control loop to the attitude control loop is minimised as much as possible. To achieve this results the values of the two matrices described above were accordingly selected so that the desired performances could be achieved.

### 3.3. Surface Deflection Logic

The purpose of this section is to describe the logic implemented to select the panels configuration providing the closest match to the required control torques coming from the quaternion feedback controller (in the case of aerodynamic pointing) or from the optimal LQR (in the case of momentum management).

Aerodynamic forces and torques in roll, pitch and yaw are given by:

$$\vec{F}_a = \begin{bmatrix} F_{a,x} \\ F_{a,y} \\ F_{a,z} \end{bmatrix} = 0.5\rho V_{rel}^2 \vec{C}_{F,A} \quad (7)$$

$$\vec{M}_a = \begin{bmatrix} M_{a,x} \\ M_{a,y} \\ M_{a,z} \end{bmatrix} = 0.5\rho V_{rel}^2 \vec{C}_{M,V} \quad (8)$$

where  $\rho$  indicates the atmospheric density,  $V_{rel}$  is the magnitude of the relative velocity vector and  $\vec{C}_{F,A}$  and  $\vec{C}_{M,V}$  are the dimensional force and momentum aerodynamic coefficients.

The computation of these last relies on a method deriving from adapting *ADBSat* [16], a panel method for aerodynamic coefficients computation available at the University of Manchester, for control purposes.

The geometry of the satellite, discretised in a 3D triangular mesh, is firstly imported. The algorithm then selects, among the mesh elements that constitute the entire surface, the ones that belongs to the main body to the one belonging to the control paddles.

Given the current angle of attack and sideslip, the local direction of the normal and tangential unit vectors is computed for each element of the surface and the dimensional normal and shear stress coefficients are computed according to the Sentman's model [42].

The contributions provided from the main body and from the control panels are computed separately. Variation of the shear stress and normal coefficients is computed for the configurations resulting from a range of possible combinations obtained considering the independent rotation of the control surfaces. The number of permutations, and thus the computational effort, is reduced assuming a constant step to span the allowed angular range. The overall dimensional aerodynamic force and torque coefficients are then computed summing the contribution coming from each element of the surface (body panels):

$$\vec{C}_{F,A} = \begin{bmatrix} C_{F,x} \\ C_{F,y} \\ C_{F,z} \end{bmatrix} = \sum_{k=1}^N (c_{\tau,k} \vec{\tau}_k - c_{p,k} \vec{n}_k) A_k \quad (5)$$

$$\vec{C}_{M,V} = \begin{bmatrix} C_{M,x} \\ C_{M,y} \\ C_{M,z} \end{bmatrix} = \sum_{k=1}^N (r_k - r_{CoM}) \times (c_{\tau,k} \vec{\tau}_k - c_{p,k} \vec{n}_k) A_k \quad (6)$$

where  $(r_k - r_{CoM})$  is the distance of each surface element from the CoM. In this way, the aerodynamic contribution coming from the main body is not treated as a disturbance but is usefully employed for control purposes. The panels configuration is finally selected computing the minimum Euclidean distance between the commanded torques and the computed control torques.

## 4. Results and Discussion

### 4.1. Shuttlecock Configuration (Aerostable)

For the aerostable shuttlecock configuration discussed in Section 2.1, feasibility of RWs momentum management and aerodynamic control in pitch & yaw were investigated.

For the momentum management task, it is assumed that the satellite is travelling a circular orbit inclined by 50° at 250 km of altitude. The RWs are actuated to counteract the external disturbances affecting the plant, such that a desired offset with regards to LVLH (5° in pitch and 3° in yaw) can be maintained. As can be seen in Figure 4, performing this task in the lower VLEO altitude range is quite demanding, due to the increased aerodynamic disturbances experienced by the satellite. The full set of RWs saturates within 25 minutes. As a

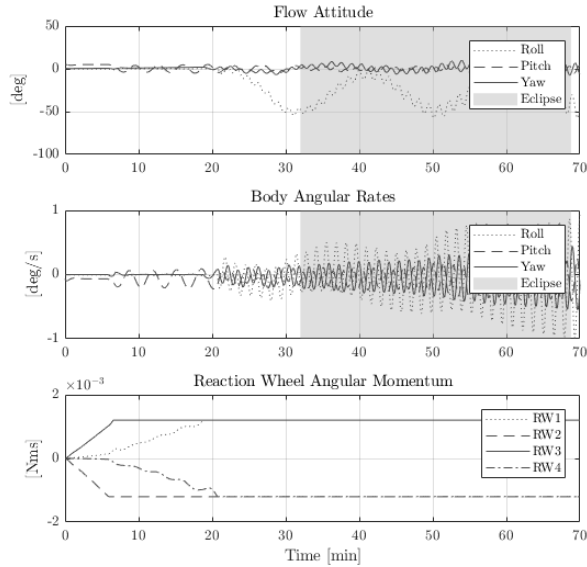


Figure 4: Time histories of the Euler angles and satellite body rates for the shuttlecock configuration when no dumping strategy for angular momentum build-up is employed. RWs saturation causes loss of system controllability and the satellite starts oscillating about the flow direction.

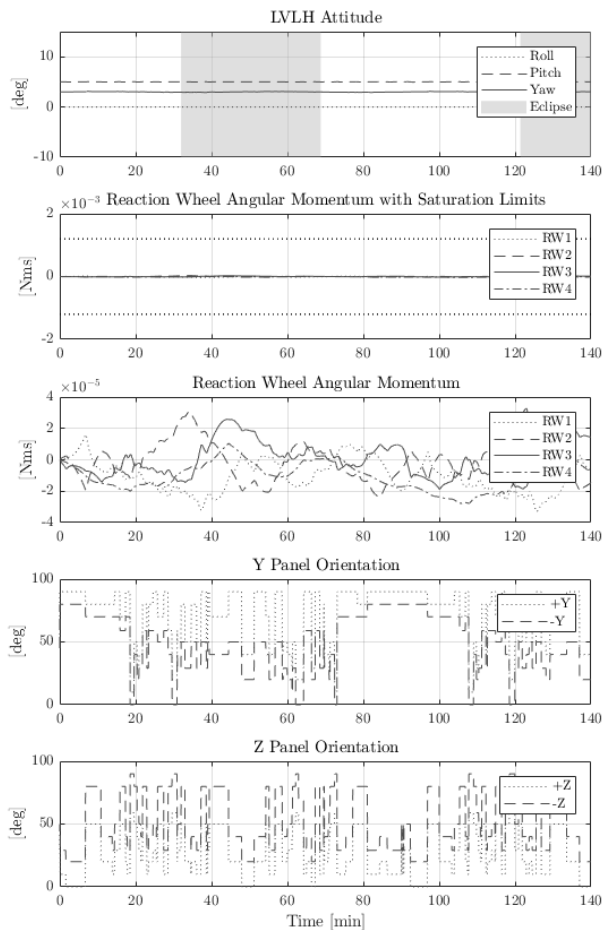


Figure 5: Performance of the aerodynamic angular momentum management task for the shuttlecock configuration.

consequence, control authority is lost and, because of its aerostable characteristic in pitch and yaw (Figure 2, first and second plot), the satellite motion shows persistent oscillation about the flow direction.

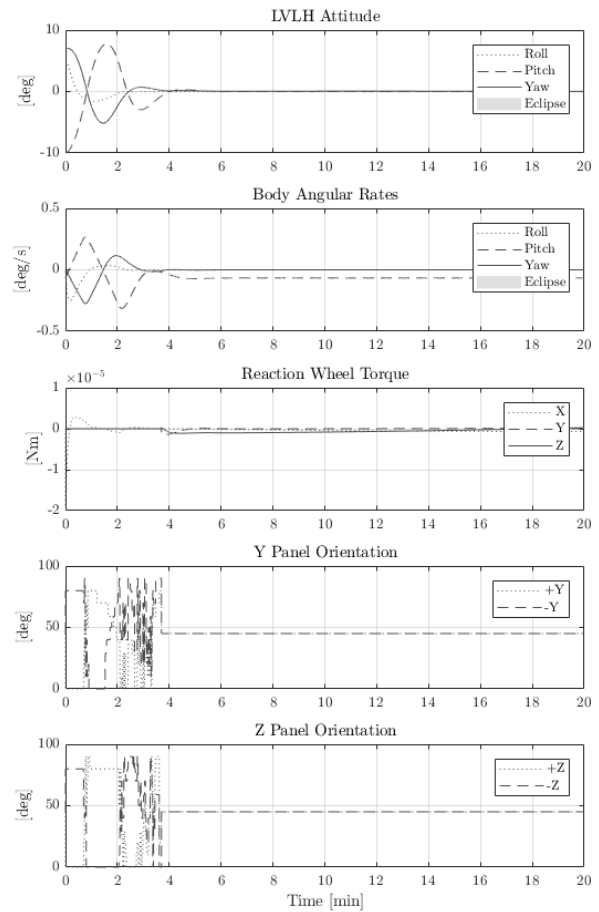


Figure 6: Performance of the aerodynamic pitch and yaw manoeuvre for the shuttlecock configuration. The satellite motion about the roll axis is controlled by the RWs.

On the contrary, when the aerodynamic management task is performed, the angular momentum stored in each wheel is kept very close to the initial null value and reasonably distant from the upper and lower saturation limits (Figure 5, second picture from the top). The third plot in Figure 5 shows the same information of the second plot from the top, but it provides an enlarged view on the variation of the angular momentum in each wheel adopting a smaller scale. Moreover, the task appears to be performed with reasonable panels activity (Figure 5, fourth and fifth plot from the top) and without interfering with the pointing task performed by the RWs in parallel (Figure 5, top). However, selection of high drag configurations may lead to a considerable increase in the orbital rate of decay. Further analysis assessing variations in the aerodynamic drag profile thus need to be performed to better evaluate the range of applicability of this manoeuvre. A possible cost-efficient solution may be

found in employing Atmospheric Breathing Electric Propulsion (ABEP) systems [47].

Feasibility of aerodynamic pointing manoeuvring in pitch and yaw has been investigated for a 280 km circular orbit inclined at 50°. Given an initial offset in roll, pitch and yaw of 5°, -10° and 7° the panels and the RWs are actuated to correct the attitude to achieve alignment with the LVLH reference frame. During the attitude stabilisation task, the aerodynamic panels succeed in correcting the attitude in pitch and yaw without any interference from the RWs. Conventional actuators provide the demanded control torque exclusively in roll (Figure 6, third plot). After the attitude has been stabilised about the desired target, the panels are moved to their nominal configuration (45°) and external environmental disturbances are compensated by the RWs. Because of the perturbation introduced by atmospheric co-rotation in yaw, the panels activity is quite intense (Figure 6, fourth and fifth plot). A possible improvement in this regard might be achievable adopting smaller gains for the quaternion feedback PID loop.

#### 4.2. Disc Configuration (Neutrally Stable)

Due to the limited controllability in pitch axis, possible employment of aerodynamic torques for stabilisation of the roll attitude has been investigated for the disc satellite geometry described in Section 2.1.

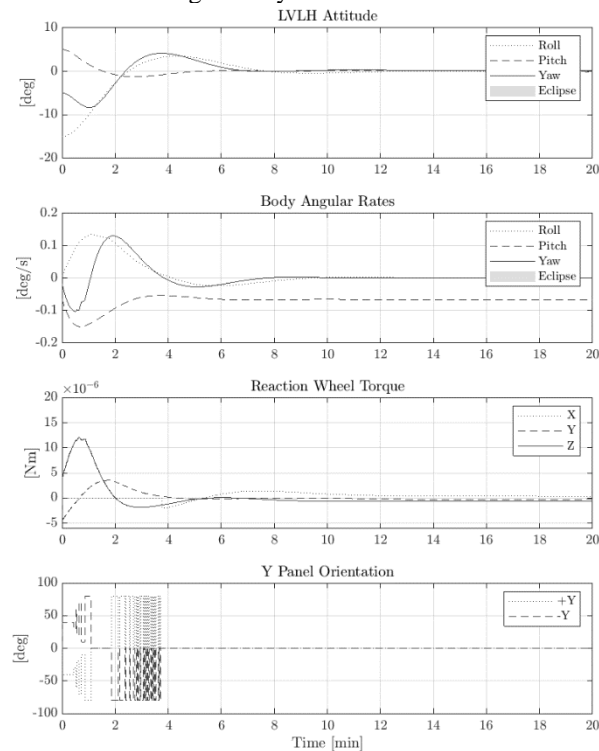


Figure 7: Performance of roll-axis aerodynamic attitude control for the disc satellite geometry. Pitch and yaw axes are controlled by means of RWs.

The results obtained for a 280 km circular orbit inclined at 50° are shown in Figure 7. The time history of the Euler angles about the LVLH reference frame (Figure 7, top) suggests that the performance of the aerodynamic task introduce some disturbances in the RWs actuation about the yaw axis. This might be explained with the fact that any asymmetries with regards to the incoming flow direction induce an aerodynamic torque in yaw as well. The attitude stabilisation in roll is achieved at the price of selecting undesired high drag panels configurations. In these conditions, the impact on the orbital rate of decay of this manoeuvre is likely to be non-negligible, especially considering the dimensions of the control panels. Improvements for this manoeuvre might be achievable adopting lower gains and more properly adjusting the controller implementation for this geometry.

#### 4.3. SOAR - Feathered Configuration (Aerostable)

A possible employment of aerodynamic torques to avoid the build-up of angular momentum in the RWs was also investigated for SOAR [32].

In this case, it was assumed that the RWs were initially commanded to restore, from an initial offset in roll, pitch and yaw, the desired alignment with the LVLH reference frame. In this way better conclusions could be derived on the effective capability of the momentum management control loop to achieve its objective without interfering with the attitude control logic. Same initial orbital conditions were also assumed to run the simulations and compare the results. Specifically, the satellite was assumed in a circular 200 km orbit inclined at 70°.

Performing the aerodynamic control loop proved to have a beneficial effect on the system (Figure 9). The initial non-null angular momentum in the wheels is properly dumped and kept very close to the null value (Figure 9, second and third plot from the top). In this way, actuators saturation is prevented (Figure 8) and control authority is preserved. Even in this case, the manoeuvre seems to be achieved with reasonable panels activity with limited, even if still present, switches between minimum and maximum drag configurations. Comparison of Figure 8 (top) and Figure 9 (top) also seems to suggest that the time separation between the two loops is wide enough to avoid interference with the attitude control task. When the aerodynamic momentum management logic is implemented (Figure 9), no appreciable difference can be noticed in the time response of the attitude controller. For this result to be confirmed, however, a more rigorous frequency response analysis is demanded and will be object of future investigations.

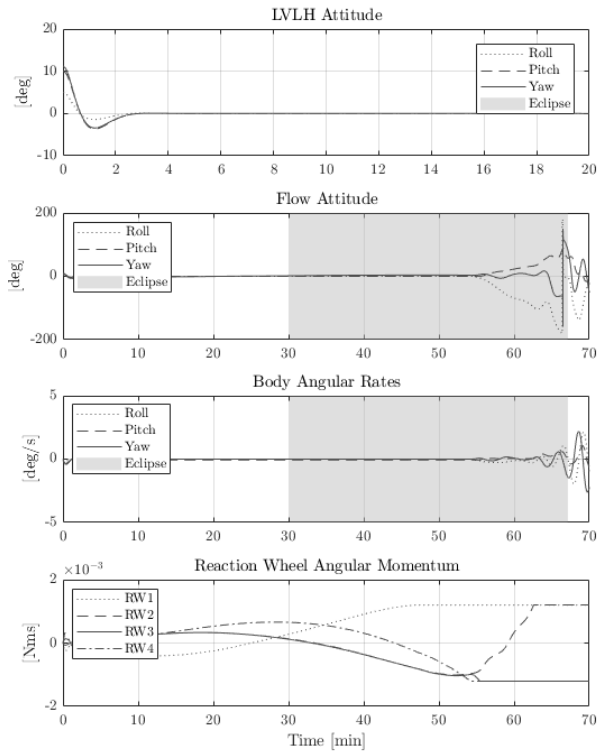


Figure 8: Time history of the attitude motion about the LVLH reference frame for the aerostable feathered configuration (SOAR) when no dumping strategy is employed. After actuators saturation, control authority is lost and undamped oscillations are observed.

The feasibility of an aerodynamic roll control manoeuvre was investigated for the feathered configuration as well. Given an initial offset in LVLH of  $5^\circ$  in roll,  $-5^\circ$  in pitch and  $5^\circ$  in yaw, the aerodynamic panels are actuated in order to stabilise the satellite attitude and to maintain a desired offset in roll with regards to the LVLH reference frame of  $-3^\circ$ . Initial orbital conditions include a null eccentricity orbit characterised by an inclination of  $50^\circ$  and an altitude of 200 km. The results shown in Figure 10 seem to be quite promising, with settling time being of the order of  $\sim 300$ s for this manoeuvre (Figure 10, top). As can be seen in the third plot from the top in Figure 10 the aerodynamic pointing manoeuvre is achieved with no interference from the RWs. As expected, during the aerodynamic pointing phase the panels algorithm preferentially selects panels counter-rotation to increase the control authority in roll (Figure 10, fourth and fifth plot). After the satellite has been stabilised about the desired pointing direction, the panels are not returned to their nominal configurations, but are still actuated to maintain the desired attitude by performing aerodynamic trim. The overall aerodynamic pointing and trim manoeuvre appears to be achievable with a reasonable control effort imposed on the panels. These results however can be improved limiting the selection of high

aerodynamic drag configurations introducing a saturation avoidance logic within the panels algorithm.

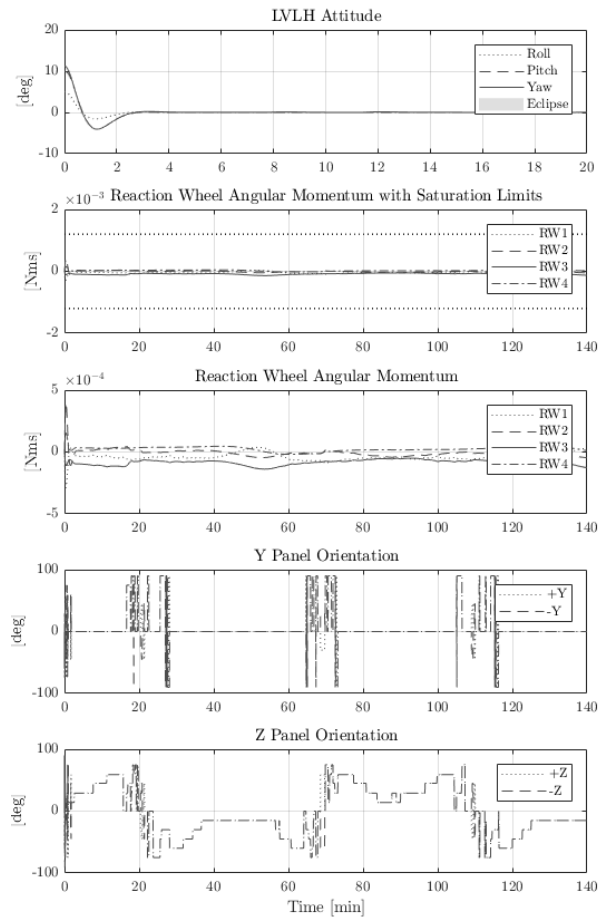


Figure 9: Performance of the aerodynamic momentum management task for the feathered configuration (SOAR). Time response separation between the attitude and the momentum management loop is investigated assuming an initial pointing manoeuvre.

Aerodynamic control of the satellite motion about the pitch and yaw axes was investigated for SOAR as well. Three-axes attitude control is achieved employing RWs exclusively for roll axis control. Even in this case, aerodynamic trim about the pitch and yaw axes was considered. The panels are accordingly actuated after the pointing control task has been achieved (Figure 11, bottom). Aerodynamic disturbances in roll are however still compensated by RWs. Simulations were run for a circular orbit at 250 km with an inclination of  $56^\circ$ . An initial offset of  $20^\circ$  in roll,  $-10^\circ$  in yaw and  $12^\circ$  was assumed with regards to LVLH.

This scenario is more challenging compared to the aerodynamic roll control one. This not only depends on the fact that control is to be provided contemporary in two axes but also on the presence of increased disturbances affecting the performance achievable with aerodynamic actuation. Satellite in non-equatorial orbits

experience disturbances in yaw due to atmosphere co-rotation with the Earth. According to this, a superior control effort is required to achieve the desired control action. This consideration is confirmed by the time histories of panels activity (Figure 11, fourth and fifth plot), which are considerably more intense than the one observed for the aerodynamic roll control case (Figure 10, fourth and fifth plot), and by the performances which are coarser in yaw. Despite the results achieved, improvements can be applied to relax the control effort demanded on the aerodynamic actuators by reducing the panels algorithm sensitivity. Small variations in the demanded control torque seem to have the effect of making the panels unnecessarily switch between the nominal configuration and the “control” configurations. Improvements may comprise the introduction of the saturation avoidance control logic mentioned before or the employment of lower gains for the quaternion feedback PID.

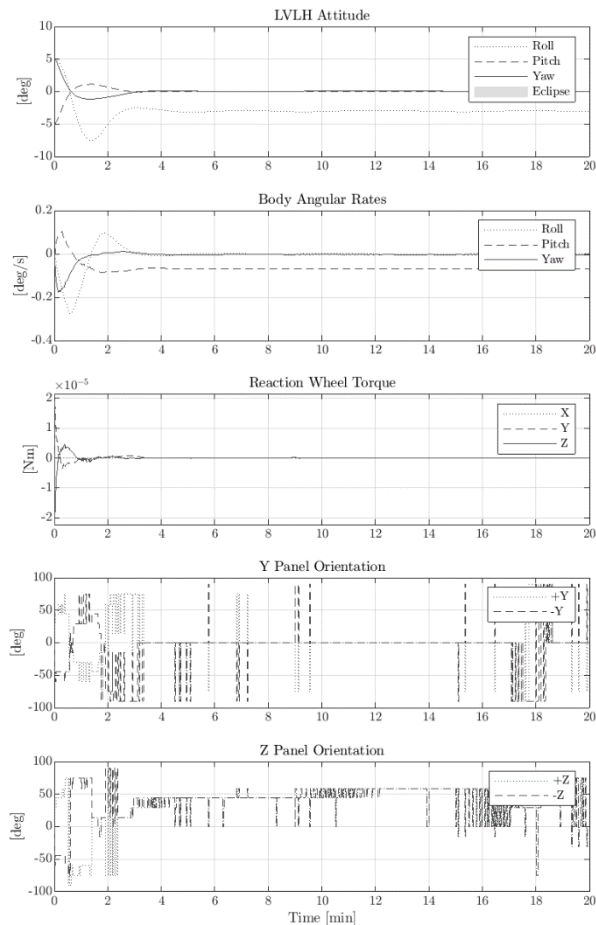


Figure 10: Performance of the combined aerodynamic roll and RWs pitch and yaw pointing manoeuvre. Aerodynamic trim about the roll axis is performed to maintain the desired offset in roll with regards to LVLH.

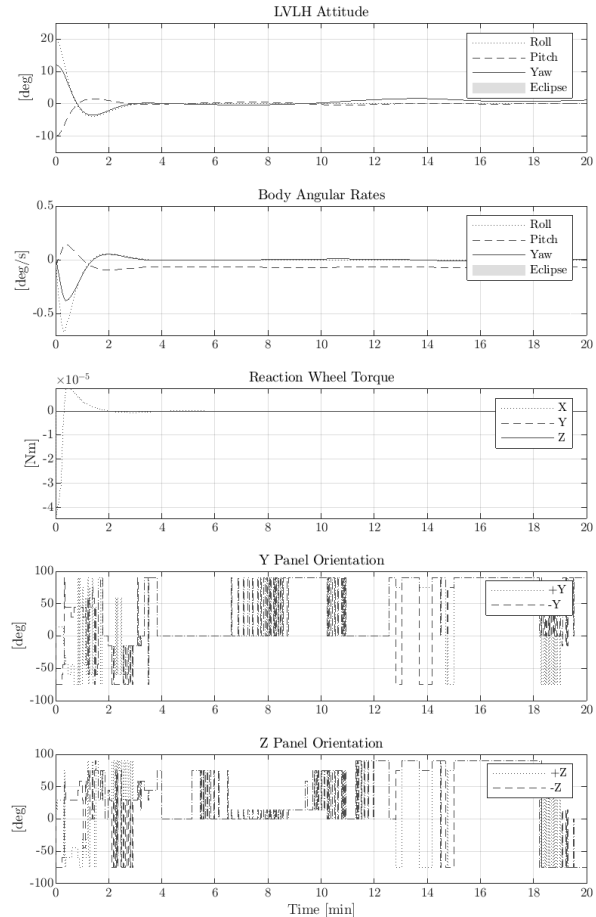


Figure 11: Performance of the aerodynamic pointing manoeuvre about the pitch & yaw axes for SOAR. Motion about the roll axis is controlled by the RWS. After the initial offset is nulled out, the aerodynamic panels are still employed to reject external disturbances in pitch and yaw.

## 5. Conclusion and Future Developments

The feasibility of a set of aerodynamic attitude control manoeuvres for operations in VLEO was investigated for two aerostable geometries (shuttlecock and SOAR) and a nominally neutrally stable configuration (disc satellite). To preserve generality, the investigation concerned varying initial orbital and pointing conditions. In particular, VLEO altitudes were selected according to the expected suitability of orbital aerodynamics control during periods of reduced solar activity [48].

The aerodynamic control manoeuvres examined comprise combined aerodynamic and RWs attitude control, aerodynamic trim and aerodynamic management of the angular momentum stored in the RWs. The control signal for the aerodynamic pointing and trim task is provided by the digital implementation of the constant gain quaternion feedback PID + intelligent integrator controller proposed by Bang et al. [45]. The momentum

management task is implemented according to a classical discrete-time infinite-horizon LQR.

The results obtained for the feathered and the shuttlecock configurations seem to be particularly promising. However, some further developments are needed. The level of detail used in the implementation of the control logics employed for this works is limited. Design and implementation of control algorithms is considerably driven by the requirements imposed on the platform considered. For this study, a description characterised by a lower specification level was preferred to favour adaption to different geometries and preserve generality. Implementation on a real platform like SOAR, however, requires addressing constraints to improve the confidence of the results obtained. Future developments will thus see the inclusion of software and hardware limitations (sensor noise and deadbands, panels deflection rates, data storage and memory etc.) as well as improvements to the logic used to determine the optimal panels configuration providing the commanded control signal. The impact of aerodynamic attitude control manoeuvres on orbit perturbation will also be addressed to better discuss the advantages achievable over the employment of conventional actuators.

#### Acknowledgements

The DISCOVERER project has received funding from the European Union's Horizon 2020 research and innovation programme under grant agreement No 737183. Disclaimer: this publication reflects only the views of the authors. The European Commission is not liable for any use that may be made of the information contained therein.

#### References

- [1] P. C. E. Roberts *et al.*, "Discoverer - Radical redesign of earth observation satellites for sustained operation at significantly lower altitudes," in *Proceedings of the International Astronautical Congress, IAC*, 2017, vol. 14, no. September, pp. 25–29.
- [2] B. Streetman, J. Shoer, and L. Singh, "Limitations of scaling momentum control strategies to small spacecraft," in *IEEE Aerospace Conference Proceedings*, 2017.
- [3] V. V. Beletsky, "Motion of an Artificial Satellite about its Center of Mass," National Aeronautics and Space Administration (NASA), U.S.A., Washington, D.C., 1965.
- [4] L. Meirovitch and F. B. J. Wallace, "On the Effect of Aerodynamic and Gravitational Torques on the Attitude Stability of Satellites.," *AIAA J.*, vol. 4, no. 12, pp. 2196–2202, 1966.
- [5] M. A. Frik, "Attitude Stability of Satellites Subjected to Gravity Gradient and Aerodynamic Torques," *AIAA J.*, vol. 8, no. 10, pp. 1780–1785, 1970.
- [6] R. Ravindran and P. C. Hughes, "Optimal Aerodynamic Attitude Stabilization of Near-Earth Satellites," *J. Spacecr. Rockets*, vol. 9, no. 7, pp. 499–506, 1972.
- [7] M. L. Psiaki, "Nanosatellite Attitude Stabilization Using Passive Aerodynamics and Active Magnetic Torquing," *J. Guid. Control. Dyn.*, vol. 27, no. 3, pp. 347–355, 2004.
- [8] S. A. Rawashdeh and J. E. Lumppp, "Aerodynamic Stability for CubeSats at ISS Orbit," *J. Small Satell.*, vol. 2, no. 1, pp. 85–104, 2013.
- [9] M. R. Drinkwater *et al.*, "The GOCE gravity mission: ESA'S first core earth explorer," *European Space Agency, (Special Publication) ESA SP*, no. SP-627. pp. 1–7, 2007.
- [10] V. A. Sarychev, S. A. Mirer, A. A. Degtyarev, and E. K. Duarte, "Investigation of equilibria of a satellite subjected to gravitational and aerodynamic torques with pressure center in a principal plane of inertia," *Celest. Mech. Dyn. Astron.*, vol. 100, no. 4, pp. 301–318, 2008.
- [11] J. Armstrong, C. Casey, G. Creamer, and G. Dutchover, "Pointing Control for Low Altitude Triple Cubesat Space Darts," in *Small Satellite Conference*, 2009, no. 202, pp. 1–8.
- [12] M. L. Gargasz, "Optimal Spacecraft Attitude Control Using Aerodynamic Torques," Air Force Institute of Technology, 2007.
- [13] J. V. Llop, P. C. E. Roberts, and Z. Hao, "Aerodynamic attitude and orbit control capabilities of the  $\Delta$ DSAT cubesat," *Adv. Astronaut. Sci.*, vol. 151, no. February, pp. 321–332, 2014.
- [14] J. Auret and W. H. Steyn, "Design of an aerodynamic attitude control system for a CubeSat," *62nd Int. Astronaut. Congr. 2011, IAC 2011*, vol. 11, no. January 2011, pp. 9009–9017, 2011.
- [15] Z. Hao and P. C. E. Roberts, "Using Aerodynamic Torques To Aid Detumbling Into an Aerostable State," *67th Int. Astronaut. Congr.*, no. September, pp. 26–30, 2016.
- [16] D. Mostaza-Prieto, "Characterisation and Applications of Aerodynamic Torques on Satellites," University of Manchester, 2017.
- [17] R. Bevilacqua and M. Romano, "Rendezvous Maneuvers of Multiple Spacecraft Using Differential Drag Under J2 Perturbation," *J. Guid. Control. Dyn.*, vol. 31, no. 6, pp. 1595–1607, 2008.
- [18] D. Pérez and R. Bevilacqua, "Differential drag spacecraft rendezvous using an Adaptive Lyapunov Control strategy," *Adv. Astronaut.*

- Sci.*, vol. 145, pp. 973–991, 2012.
- [19] L. Dell’Elce and G. Kerschen, “Optimal propellantless rendez-vous using differential drag,” *Acta Astronaut.*, vol. 109, pp. 112–123, 2015.
- [20] G. B. Palmerini, S. Sgubini, and G. Taini, “Spacecraft orbit control using air drag,” in *International Astronautical Conference*, 2014, no. January 2005.
- [21] O. Ben-Yaacov and P. Gurfil, “Long-Term Cluster Flight of Multiple Satellites Using Differential Drag,” *J. Guid. Control. Dyn.*, vol. 36, no. 6, pp. 1731–1740, 2013.
- [22] C. Lambert, B. S. Kumar, J. F. Hamel, and A. Ng, “Implementation and performance of formation flying using differential drag,” *Acta Astronaut.*, vol. 71, pp. 68–82, 2012.
- [23] H. Leppinen, “Deploying a single-launch nanosatellite constellation to several orbital planes using drag maneuvers,” *Acta Astronaut.*, vol. 121, pp. 23–28, 2015.
- [24] J. Virgili, P. C. E. Roberts, and N. C. Hara, “Atmospheric Interface Reentry Point Targeting Using Aerodynamic Drag Control,” *J. Guid. Control. Dyn.*, vol. 38, no. 3, pp. 403–413, 2015.
- [25] S. Omar and R. Bevilacqua, “Guidance, navigation, and control solutions for spacecraft re-entry point targeting using aerodynamic drag,” *Acta Astronaut.*, 2018.
- [26] M. Horsley, S. Nikolaev, and A. Pertica, “Small Satellite Rendezvous Using Differential Lift and Drag,” *J. Guid. Control. Dyn.*, vol. 36, no. 2, pp. 445–453, 2013.
- [27] X. Shao, M. Song, D. Zhang, and R. Sun, “Satellite rendezvous using differential aerodynamic forces under J2 perturbation,” *Aircr. Eng. Aerosp. Technol.*, vol. 87, no. 5, pp. 427–436, 2015.
- [28] B. Smith, R. Boyce, L. Brown, and M. Garratt, “Investigation into the Practicability of Differential Lift-Based Spacecraft Rendezvous,” *Journal of Guidance, Control, and Dynamics*, vol. 40, no. 10, pp. 1–8, 2017.
- [29] R. Sun, J. Wang, D. Zhang, Q. Jia, and X. Shao, “Roto-Translational Spacecraft Formation Control Using Aerodynamic Forces,” *J. Guid. Control. Dyn.*, vol. 40, no. 10, pp. 2556–2568, 2017.
- [30] P. Moore, “The effect of Aerodynamic Lift on Satellite Orbits,” *Planet Sp. Sci.*, vol. 33, no. 5, pp. 479–491, 1985.
- [31] C. Traub, G. H. Herdrich, and S. Fasoulas, “Influence of energy accommodation on a robust spacecraft rendezvous maneuver using differential aerodynamic forces,” *CEAS Sp. J.*, 2019.
- [32] N. H. Crisp *et al.*, “SOAR - Satellite for orbital aerodynamics research,” in *Proceedings of the International Astronautical Congress, IAC*, 2018.
- [33] F. L. Markley and J. L. Crassidis, *Fundamentals of spacecraft attitude determination and control*. 2014.
- [34] M. F. Larsen and J. W. Meriwether, “Vertical winds in the thermosphere,” *J. Geophys. Res. Sp. Phys.*, vol. 117, no. 9, pp. 1–10, 2012.
- [35] E. Doornbos and H. Klinkrad, “Modelling of space weather effects on satellite drag,” *Adv. Sp. Res.*, vol. 37, no. 6, pp. 1229–1239, 2006.
- [36] J. M. Picone, A. E. Hedin, D. P. Drob, and A. C. Aikin, “NRLMSISE-00 empirical model of the atmosphere: Statistical comparisons and scientific issues,” *J. Geophys. Res. Sp. Phys.*, vol. 107, no. A12, pp. 0–16, 2002.
- [37] A. E. Hedin, N. W. Spencer, and T. L. Killeen, “Empirical global model of upper thermosphere winds based on atmosphere and dynamics explorer satellite data,” *J. Geophys. Res.*, vol. 93, no. A9, pp. 9959–9978, 1988.
- [38] A. E. Hedin *et al.*, “Revised global model of thermosphere winds using satellite and ground-based observations,” *J. Geophys. Res.*, vol. 96, no. A5, pp. 7657–7688, 1991.
- [39] D. P. Drob *et al.*, “An empirical model of the Earth’s horizontal wind fields: HWM07,” *J. Geophys. Res. Sp. Phys.*, vol. 113, no. 12, pp. 1–18, 2008.
- [40] European Cooperation For Space Standardization (ECSS), “ECSS-E-ST-10-04C Space environment,” Noordwijk, The Netherlands, 2008.
- [41] D. Mostaza Prieto, B. P. Graziano, and P. C. E. Roberts, “Spacecraft drag modelling,” *Prog. Aerosp. Sci.*, vol. 64, pp. 56–65, 2014.
- [42] L. H. Sentman, “Free molecule flow theory and its application to the determination of aerodynamic forces,” Sunnyvale, California, 1961.
- [43] B. A. Banks, K. K. de Groh, and S. K. Miller, “Low Earth Orbital Atomic Oxygen Interactions With Materials,” *NASA/TM-2004-213400*, no. November. Glenn Research Center, Cleveland, Ohio, pp. 1–19, 2004.
- [44] K. Moe and M. M. Moe, “Gas-surface interactions and satellite drag coefficients,” *Planet. Space Sci.*, vol. 53, no. 8, pp. 793–801, 2005.
- [45] H. Bang, M. J. Tahk, and H. D. Choi, “Large angle attitude control of spacecraft with actuator saturation,” *Control Eng. Pract.*, vol. 11, no. 9, pp. 989–997, 2003.
- [46] B. Wie, H. Weiss, and A. Arapostathis,

- “Quaternion feedback regulator for spacecraft eigenaxis rotations,” *J. Guid. Control. Dyn.*, vol. 12, no. 3, pp. 375–380, 1989.
- [47] F. Romano, T. Binder, G. Herdrich, S. Fasoulas, and T. Schönherr, “Air-Intake Design Investigation for an Air-Breathing Electric Propulsion System,” *Int. Electr. Propuls. Conf.*, pp. 1–27, 2015.
- [48] N. H. Crisp *et al.*, “Demonstration of Aerodynamic Control Manoeuvres in Very Low Earth Orbit using SOAR (Satellite for Orbital Aerodynamics Research),” *70th Int. Astronaut. Congr.*, no. October, pp. 21–25, 2019.